Published in final edited form as:
J Theor Biol. 2009 April 7; 257(3): 430–437. doi:10.1016/j.jtbi.2008.12.011.

A quantitative examination of the role of cargo-exerted forces in axonal transport

Cassie S. Mitchell and **Robert H. Lee**
Laboratory for Neuroengineering, Wallace H. Coulter Department of Biomedical Engineering, Georgia Institute of Technology and Emory University, Atlanta, GA, USA

Abstract

Axonal transport, via molecular motors kinesin and dynein, is a critical process in supplying the necessary constituents to maintain normal neuronal function. In this study, we predict the role of cooperativity by motors of the same polarity across the entire spectrum of physiological axonal transport. That is, we examined how the number of motors, either kinesin or dynein, working together to move a cargo, results in the experimentally determined velocity profiles seen in fast and slow anterograde and retrograde transport. We quantified the physiological forces exerted on a motor by a cargo as a function of cargo size, transport velocity, and transport type. Our results show that the force exerted by our base case neurofilament (D_{NF}=10nm, L_{NF}=1.6μm) is ~1.25pN at 600nm/s; additionally, the force exerted by our base case organelle (D_{Org}=1μm) at 1,000nm/s is ~5.7pN. Our results indicate that while a single motor can independently carry an average cargo, cooperativity is required to produce the experimental velocity profiles for fast transport. However, no cooperativity is required to produce the slow transport velocity profiles; thus, a single dynein or kinesin can carry the average neurofilament retrogradely or anterogradely, respectively. The potential role cooperativity may play in the hypothesized mechanisms of motoneuron transport diseases such as Amyotrophic Lateral Sclerosis (ALS) is discussed.

Keywords

neurofilament; axoplasm; microtubule; computational model; cooperative transport; drag force

Introduction

With axons being unable to manufacture their own proteins, axonal transport is a critical process responsible for providing essential cellular parts and materials throughout the entire axon and for returning molecules destined for degradation back to the lysosomes in the soma (Sabry et al., 1995). For a review of axonal transport, see (Goldstein and Yang, 2000). With numerous recent experimental investigations pointing to the potential role of axonal transport in such devastating motoneuron diseases as Amyotrophic Lateral Sclerosis (ALS) (Pantelidou et al., 2007; Rao and Nixon, 2003; Zhang et al., 2007), Spinal Muscular Atrophy (Briese et al., 2005), and Charcot-Marie-Tooth disease (Brownlees et al., 2002; Lupski, 2000), there is an ongoing effort to reveal the pathological mechanisms resulting in associated transport defects. However, many questions remain regarding the physiological mechanisms of axonal transport,

corresponding, E-mail: rlee2@emory.edu, Phone: 404-894-4484 Fax: 404-385-5044.

and the answers to these questions lie in the path of our full understanding of transport-related diseases.

One such question has been the identification and subsequent characterization of cooperative movement of cargos by multiple motors, which equally share load force. That is, how many motors does it take to move a cargo, and if and how is cooperativity affected by cargo type/size and transport speed? Although it has been suggested that cooperativity does exist (Ashkin et al., 1990; Gross et al., 2002; Klumpp and Lipowsky, 2005; Kural et al., 2005), experimental validation has proven difficult. Most work examining cooperativity has focused on the cooperative movement between motors of opposite polarity (Gross et al., 2002; Kural et al., 2005) (i.e. dynein and kinesin moving a cargo in a concerted fashion) rather than the cooperativity of multiple same polarity kinesins or dyneins working to move a cargo either anterogradely or retrogradely, respectively. While optical trap experiments have characterized the maximum forces a molecular motor can withstand (Ashkin et al., 1990; Coppin et al., 1995; Gross et al., 2002), little is known as to how these measured forces compare to what physiological forces a motor may experience when carrying cargos. Therefore, it has been difficult to determine the number of motors necessary to overcome the forces imposed by moving a given cargo.

In this study, we quantitatively examine the role of same polarity multi-motor cooperativity as a function of cargo type/size, transport velocity, and transport type. We determine the forces imposed on a molecular motor under a wide physiological range of parameters. Using these calculated forces in combination with an adapted version of an experimentally-derived kinetic model (Craciun et al., 2005), which accurately describes the appropriate states of the motor as it processes along the microtubule, we were able to quantify and characterize molecular motor cooperativity over established, experimentally determined, fast (200–400 mm/day) and slow transport (0.3–8 mm/day) ranges (Brown, 2000; Brown et al., 2005; Kural et al., 2005; Shea and Flanagan, 2001; Wang et al., 2000). Our results indicate under certain transport scenarios, cooperativity is necessary to achieve fast transport, but its role in slow transport is minimal. Furthermore, our results suggest the potential for a substantial impact of cooperativity in transport disease pathologies.

Methods

The two most characterized cargo types are the neurofilaments, which undergo slow transport, and mitochondria, which undergo fast bi-directional transport. Thus, we choose to focus the majority of our study on these two cargo populations. Table 1 lists the experimental velocity transport ranges for most common types of hypothesized and known cargo types.

The general strategy was to determine the force imposed by various cargo types and to use this information to determine the number of bound motors required to move a specific cargo type at transport velocity ranges that match those determined experimentally using optical traps (Coppin et al., 1995). This general strategy is based on: 1) determining the force imposed by the cargo by calculating the drag force as a function of velocity and cargo geometry; 2) assuming the drag force is equivalent to the maximum force exerted by the cargo on the molecular motor; and 3) determining the velocity distributions for various cargo sizes and types undergoing transport by a specified number of bound motors using the appropriate transport kinetics to describe the interaction of the molecular motors with the microtubule for each specific transport type.

Drag Force Calculation

The drag force imposed by a cargo was represented by simplified equations derived from the Stokes-Einstein equation for a particle at a low Reynolds number, $Re \ll 1$ (Berg, 1993; Truskey

et al., 2003). The relationship of drag force, (F_D), to velocity (V) for an arbitrarily shaped particle is described by Equation 1 where f is the frictional coefficient:

$$F_D = f \cdot v \qquad \text{Eqaution 1}$$

The geometry-specific frictional coefficient, f, for a cylindrical neurofilament is calculated using Equation 2 (Truskey et al., 2003) where L_{NF} is length, D_{NF} is diameter, and μ is viscosity of the surrounding cytoplasm (sometimes referred to as the axoplasm).

$$f = \frac{4\pi\mu L_{NF}}{\ln(L/(D_{NF}/2)) + 0.193} \qquad \text{Eqaution 2}$$

Organelles carried in fast transport, such as mitochondria, are known to have a spherical geometry and were modeled as simple spheres. The simplified geometry-specific frictional coefficient for a spherical organelle is given by Equation 3 (Berg, 1993) where D_{org} is the diameter of the organelle.

$$f = 6\pi\mu(D_{org}/2) \qquad \text{Eqaution 3}$$

The maximum allowable drag force is calculated by multiplying the number of bound motors, N_B, by their maximum force, F_s, for the appropriate motor type (Equation 4). A motor's maximum force can be assumed to be its measured "stall" force. (The stall force is the opposing force needed to slow a motor to zero velocity.) The stall force has been experimentally determined to be ~1.2 pN for dynein (Gao, 2006; Schmitz et al., 2000) and ~5.65 pN for kinesin (Coppin et al., 1995; Kural et al., 2005) at physiological concentrations of available ATP; thus, we use these average experimental values of F_s in the this study.

$$F_{D_{MAX}} = F_s \cdot N_B \qquad \text{Eqaution 4}$$

The velocity of an individual cargo was determined by substituting the maximum drag force ($F_{D,MAX}$) in Equation 4 for the drag force (F_D) in Equation 1. Thus, the cargo velocity calculation is given by Equation 5.

$$V = F_{D_{MAX}} / f \qquad \text{Eqaution 5}$$

Determination of drag force parameters

Much care was taken to obtain values for all four of the drag force calculation parameters over their physiological ranges (see Table 2). Three such aforementioned parameters describe cargo geometry: the diameter of either an organelle (D_{org}) or a neurofilament (D_{NF}) and the length of a neurofilament (L_{NF}). Neurofilaments have been determined to be approximately 10nm in diameter (Lupski, 2000), but their lengths have not yet been precisely determined. Neurofilaments are thought to be transported in their polymerized form, which implies that they could reach great lengths, ~1–3μm (Brown, 1998;Trivedi et al., 2007;Wagner et al., 2004), with an average around 1.8 μm. Neurofilaments contain "branches" or "side arms" due to the neurofilament medium and heavy subunits (NF-M and NF-H, respectively), which

provide the cross-linking and phosphorylation interaction and regulation sites (Marszalek et al., 1996). However, we chose to assume a simpler, plain cylindrical shape to model the neurofilament geometry. As shown in the results, increasing the diameter to include the side arms has a minimal impact on the calculated force. The size of fast transport particles can vary from the nanometer to micrometer scale. The average size of mitochrondria is about 1 μm. Note that 'reasonable' instantaneous velocities (i.e. velocities < ~3000 nm/s over a time period of ~ 5 seconds as shown by an invivo study slow transport of neurofilaments (Brown et al., 2005) and by an invivo study of quantum dot labeled fast transport (Yoo et al., 2008)) can only be attained with organelle diameters greater than approximately 200 nm. Diameters smaller than this are assumed to be kinetically limited, rather than force limited and thus are not included in this study.

The fourth drag force parameter is the viscosity of the surrounding cytoplasm (or axoplasm). Due to the anisotropic properties of the cytoplasm, a precise determination of viscosity is very difficult. Bulk cytoplasm contains ~20% protein, which contributes to physical properties that mimic a weakly viscoelastic gel (Hou et al., 1990). This gel is a result of the combined properties of the actin protein network, which provides cytoskeletal structure and support and the cytoplasmic fluid itself which is about 80% water (Hou et al., 1990). Cytoplasmic viscosity measurements that do not include the protein/actin component can be as small as 0.06 Poise (Haak et al., 1976). However, viscosity measurements which look at the total cytoplasmic viscosity (actin + fluid) can be orders of magnitude higher (Keller et al., 2003). Using data from (Keller et al., 2003), we estimate the viscosity to be about 6 Poise (or 0.6 Pa•s).

Motor to microtubule binding kinetics

We adapt transport kinetics described by Craciun et al. (2005) in order to obtain physiological average velocities that take into account different possible motor-microtubule kinetic states. This scheme, as shown in Figure 1, describes both retrograde and anterograde transport using the following five states: S_O) off-track, paused; S_{KP}) kinesin, on-track, paused; S_{DP}) dynein, on-track, paused; S_{KM}) kinesin, on-track, moving anterogradely; S_{DM}) dynein, on-track, moving retrogradely. The scheme is such that a cargo must disengage from the track before switching directions, and it must pass through an on-track paused state before moving.

We implement the kinetic scheme using event-based simulation (Banks et al., 2005), a method that speeds simulation time by avoiding unnecessary repetitive calculations by predicting how long a cargo will remain in the same state. The expected duration of each possible state, t_{state}, is calculated by multiplying the inverse of the state's rate constant, k, by the natural log of a random number, *rand*, in the range 0–1 exclusive giving:

$$t_{state} = -1/k \cdot \ln(rand) \qquad \text{Eqaution 6}$$

The form of Equation 6 is chosen to fit the exponential first order process that is apparent in experimental data (Wang and Brown, 2001) as published in Table 1 of (Brown et al., 2005). The state with the shortest duration becomes the next state for that cargo. Based on the duration of the cargo's current state and the current time in the simulation, a sorted list determines when each cargo should be re-evaluated so that not every cargo need be evaluated at every time step.

Rate constants for slow transport were adjusted from those originally published by (Craciun et al., 2005) (i.e. λ and γ and were varied while all other parameters were held constant) to fit our model implementation and still match the original outputs (for derivation details, see (Craciun et al., 2005)). Briefly, γ and λ were tuned such that the histogram of cargo velocities for a neurofilament matched those presented in Table 1 of (Brown et al., 2005) for an equivalent simulated period of 4.74 seconds, giving $\gamma = 2.5$ and $\lambda = 0.1$.

The same Craciun kinetic model, with different rate constants, was used to obtain fast transport kinetics. It has been shown that slow transport is 'slow' because of the long on- and off-track pauses that occur over a longer period, making the actual movement of slow transport fast, but asynchronous and intermittent (Brown, 2000; Brown et al., 2005). Thus, the instantaneous velocity ranges during the moving states (S_{KM} and S_{DM}) for transient movement during slow transport are relatively similar to that of fast transport, but the amount of time spent in the paused and off-track states (λ and γ respectively; see figure 1) differs.

Another potential difference between slow and fast transport Craciun kinetics concerns the directionality of cargos. In the case of slow transport, the directionality of neurofilaments was found to be *net* anterograde with a ratio of anterograde to retrograde movement approximately 2:1, resulting in a kinetic rate coefficient specifying the directionality to be 69/31 as illustrated in Figure 1. In the case of fast transport of mitochondria, the net directionality is a function of axonal growth. During axonal growth the direction of movement is net anterograde, and in non-growing periods the direction of movement is net retrograde (Morris and Hollenbeck, 1993). Nonetheless, the directionality ratio was similar to that of slow transport for separate net anterograde and retrograde populations. That is, the rate of anterograde to retrograde movement is on average about 2:1 for a net anterograde population and approximately 1:2 for a net retrograde population (Morris and Hollenbeck, 1993). To take into account this difference in directionality, *net* anterograde and *net* retrograde populations were modeled separately for fast axonal transport.

Given that the directionality rate coefficients for fast transport are known, the kinetics described by the Craciun model can be made fast by simply adjusting the rate constants governing how long a cargo spends in the paused or off-track states (λ and γ). To simulate fast transport, the rate parameters, λ and γ, were adjusted or 'tuned' (i.e. λ and γ and were varied while all other parameters were held constant) until the average velocity of a population of cargos with a single bound motor ($N_B = 1$) over the duration of the entire simulation matched that seen experimentally (Visscher et al., 1999). These adjustments ($\gamma = 0.2$ and $\lambda = 10$) increase the amount of total time spent in the moving states and decrease the amount of overall time spent in the paused and off-track states. Using these adjustments, the fast transport of net anterograde and net retrograde populations were modeled. This adjustment of kinetic parameters to match fast experimental transport data was based on neurofilament cargos undergoing net anterograde fast transport both for consistency and in an attempt to keep the cargo sizes small (neurofilament cargos produce forces that are equivalent to ~250 nm spherical or organelle cargo). Keeping the cargo sizes on the smaller end of the physiological and force-limited range kept the analysis of kinetics to be independent from that of cooperativity. Rate constants were tuned such that the net anterograde population of cargos, each being carried by a single motor ($N_B = 1$), had an average velocity equal to that shown by analysis of single kinesin molecules undergoing fast transport as studied under molecular clamp (~ 1 μm/s) (Visscher et al., 1999).

Model Implementation

The entire model, including the calculation of drag force and motor kinetics is implemented in MATLAB 2007a (The Mathworks, Inc.). Simulations were repeated for 1,000 cargos to obtain the histogram velocity profiles. For validation purposes, the simulated time frame was 4.74 (or ~5) seconds, a time frame that is equivalent to the time frames and resolution of previous published experimental studies (Ashkin et al., 1990; Gross et al., 2002; Wang et al., 2000).

Results

Cargo imposed forces (i.e. drag force)

Geometry, viscosity, and velocity data taken from experimental studies were used to determine the average drag force for both neurofilaments (typical slow transport cargos) and organelles (typical fast transport cargos). Note that from here forward, we use “drag force” and “cargo imposed force” interchangeably (see assumptions in the Methods). The drag force exerted by the base case neurofilament (D_{NF}=10nm, L_{NF}=1.6μm) is ~1.25pN at 600nm/s; additionally, the drag force exerted by the base case organelle (D_{Org}=1μm) at 1,000nm/s is ~5.7pN. These values are functionally significant in that they align well with the experimentally determined maximum forces of kinesin and dynein (see Discussion).

Figure 2 shows the relationship between the drag force and each parameter over its physiological range based on Equation 2 for neurofilaments and Equation 3 for organelles. In general, the physiological range of calculated drag force is between 0.1–4 pN for a neurofilament and between and 0.3–10 pN for an organelle. Viscosity has a potentially wide range depending on how it is measured (see determination of drag force parameters in the Methods). However, viscosities lower than ~5 Poise or greater than ~7 Poise results in highly unrealistic velocity distributions (not shown). As for geometry, the spherical organelle diameter has the largest impact. Notably, increasing the diameter of the cylindrical neurofilament to include the side arms of NF-H subunits does not have a dramatic effect on the resulting drag force, increasing it by only ~25%, thereby justifying the simpler cylindrical geometry excluding side arms (see Methods). While the physiological range of transport is, for the most part, between 1,000–3,000 nm/s, speeds up to 12,000 nm/s for a peroxisome have been observed (Kural et al., 2005), a velocity that would result in a ~68 pN drag force.

Effect of Cooperativity

Using the force values calculated for organelles and neurofilament transport along with the appropriate fast or slow transport kinetics, the number of bound molecular motors required to achieve a velocity profile matching experimentally measured velocity ranges was determined for each transport type: fast anterograde and retrograde, ‘bi-directional’ anterograde and retrograde, and ‘net anterograde’ slow transport. The number of required bound motors to obtain the average velocity for each form of fast transport is illustrated in Figure 3 and summarized in Table 3.

Fast transport—For fast bidirectional anterograde transport of a 1 μm organelle (Figure 3A), 2 motors results in an average velocity of 0.68 μm/s (59 mm/day) with a standard deviation of 0.11 μm/s (9 mm/day). For 3 motors (not shown) the average velocity is 0.97 μm/s (80 mm/day) with a standard deviation of 0.15 μm/s (13 mm/day). Thus, both 2 and 3 motors result in profiles that could be classified as being within the experimentally observed range of 50 to 100 mm/day if the experimentally observed range is assumed to include at least the middle two standard deviations (i.e. +/− 1 standard deviation). Likewise, 11–14 motors result in profiles that could be classified as being within the experimentally observed range of 50 to 100 mm/day for fast bidirectional retrograde transport of a 1 μm organelle (see Figure 3B). For fast anterograde and retrograde transport (200–400 mm/day) of a 200 nm organelle, the number of motors required is 2–3 and 9–12, respectively (Figures 3C and 3D). Interestingly, the number of bound motors for an anterogradely moving 200 nm organelle is comparable to what has been suggested experimentally for amoeba mitochondria of approximately the same size (Ashkin et al., 1990). In general, the results in Table 3 illustrate that a substantially lesser amount of cooperativity is required for fast anterograde versus retrograde transport. That is, a higher degree of cooperativity is required to retrogradely move cargos, particularly larger cargos, at the top fast transport speeds. The large calculated values for retrograde cooperativity

suggest a functional role for the lower stall force of dynein in sorting and maintaining proper transport directionality and give clues as to the types and characteristics of retrogradely-bound cargos (see Discussion).

Slow transport—Slow transport of neurofilaments is net anterograde, with movements being in the anterograde direction 69% of the time and in the retrograde direction 31% of the time (Brown et al., 2005; Craciun et al., 2005), but due to the amount of time spent paused and off-track, there is little to no distinction between 'retrograde' and 'anterograde' populations. The slow transport velocity profile for a population of neurofilaments (L_{NF}=1.6 μm and D_{NF} = 10nm) is equivalent the profiles published in (Brown et al., 2005), with 83% of the motors being paused over a simulated period of 4.74 seconds (Figure 4). Across the physiological range of neurofilament lengths (~1–3 μm), no cooperativity is required (i.e. within two standard deviations of experimental data). However, the best fit to experimental data is obtained when a fraction of neurofilaments have two motors bound, particularly for neurofilaments lengths ≥2 μm. For example, to duplicate the velocity distribution given in (Brown et al., 2005) for a population of 2 μm neurofilaments, transport is accomplished with a single motor ~67% of the time and two motors ~33% of the time.

Summary of Predictions

As we have shown, using a computational model that includes kinetics and cooperativity, we are able to reproduce the experimentally determined velocity ranges for the various fast and slow transport types. However, an important aspect of any model is the ability to make specific predictions regarding previously uncharacterized dynamics or functions. Here we use our simulations to predict the following:

1. The physiological range of values for both velocity and geometry have substantial impacts on the cargo drag force (Figure 2). While there is a large potential range for cytoplasmic viscosity, which in turn would drastically alter the calculated drag forces, only the smaller simulated range (Figure 2) has an impact that mimics physiological forces that match experimental velocities.
2. Cooperativity is required by motors of the same polarity to produce fast transport profiles (Figure 3). Thus, multiple motors are required for typical physiological fast transport.
3. No cooperativity is required by motors of the same polarity to produce slow transport profiles (Figure 4). Neurofilaments are carried anterogradely or retrogradely by a single kinesin or dynein most of the time.

Discussion

In this study, we provide an initial quantitative characterization of cooperativity, including an assessment of the forces experienced by the molecular motors kinesin and dynein under physiological ranges of cargo type/size and transport velocity. Our results indicate that kinesin and dynein are ideally suited to transport the *average* cargo at the *average* speed for slow transport and *smaller* cargos at the *average* speed for fast transport without the need for cooperativity. However, cooperativity is crucial, particularly in fast transport, to obtain the full range of velocities observed experimentally. These results not only indicate possible functional outcomes of cooperativity in the regulation and maintenance of normal physiological transport, but also reveal its potential role in hypothesized pathological mechanisms of transport deficits associated with diseases such as ALS. The details and implications of these results are discussed below.

Physiological role of cooperativity

Our results show that the drag force exerted by our base case neurofilament and organelle are 1.25 pN and 5.7 pN, respectively. It is likely no coincidence that these forces are near the experimental stall forces for a single dynein and kinesin, 1.2 pN (Gao, 2006) and 5–6 pN (Coppin et al., 1995), respectively. Thus, it would seem that the "stall" or maximum generated forces are such that a single motor is generally able to carry the average neurofilament load; a single kinesin can move an average organelle at speeds up to 1 μm/s while a single dynein reaches top speed with such an organelle cargo at ~200 nm/s. These results support the experimental evidence that slow transport of neurofilaments is accomplished by a single motor of each type (Howard et al., 1989), i.e. one kinesin for anterograde movement and one dynein for retrograde movement, and that larger organelle cargos undergoing fast transport require multiple motors (Kural et al., 2005), i.e. multiple kinesins or dyneins for anterograde or retrograde movement, respectively. This inherent ability of a single motor to be able to move a load is likely a key factor helping to maintain axonal traffic by preventing the pile-up of motors and/or cargos, which would occur if multiple motors would be required to move every single cargo. Though cooperativity is not required to simply move an average cargo, it is required to move cargos at higher rates of speed and larger cargo sizes, particularly in the retrograde direction. The ability of cooperativity to alter and organize the speeds of various cargo types traveling in a specific direction could be quite functional, serving as a potential 'pacing' mechanism to prioritize which cargos are moving when and how fast.

The approximately five-fold difference between the stall forces of dynein and kinesin accounts for the equivalent linear increase in cooperativity that is required for dynein compared to kinesin. This difference could have a functional purpose in that it helps the directionality and speeds of the transported cargos, aiding in transport kinetics. That is, a bigger cargo headed anterogradely will tend to remain headed anterogradely due to the larger number of bound dyneins that would be required for it to reverse direction (i.e. the availability of dynein and their probability of binding is rate-limiting to the reverse reaction). However, it could be that this difference simply indicates that, in general, retrogradely transported cargos are smaller. It seems rather unlikely, for example, that 14 dyneins would routinely bind to carry a larger cargo such as an organelle at top fast transport speeds of 400 mm/day. Such extreme necessity for cooperativity involving very high-order kinetics would likely become an energetic burden resulting in possible local ATP depletion and ultimately a motor-limited transport process that would be extremely erratic and slow. Having smaller retrograde cargos would seem to make intuitive sense given that most retrograde bound cargos are hypothesized to be destined to the lysosomes for degradation. Thus, these cargos may have already undergone some preliminary form of degradation into smaller subunits or pieces at the synapse or in the axon.

An interesting possibility is that the difference between fast and slow transport is not attributable to kinetics at all, but rather is based entirely on cooperativity. A simple calculation indicates that fast transport speeds can be attained with slow transport kinetics applied to multiple motors acting cooperatively. However, further investigation of the interactions of multiple motors and their resulting kinetics will be necessary to decisively determine whether cooperativity can solely account for the differences seen in fast and slow transport.

Pathological role of cooperativity

The apparent role of cooperativity and its necessity, particularly in fast transport and in carrying larger cargos, increases the negative impact of potential hypothesized pathological mechanisms associated with disease-related transport deficits. For example, some experimental models of ALS have been linked to mutations in either dynein or kinesin (Brownlees et al., 2002; Hafezparast et al., 2003; Hurd and Saxton, 1996; Teuchert et al., 2006), which render a subpopulation of the motors ineffective (Jiang et al., 2005; Pantelidou et al., 2007; Rao and

Nixon, 2003). A decrease in the number of functional motors available for transport would decrease the functional capability of cooperativity as transport became motor-limited, resulting in subsequent transport deficits. In fact, one hypothesis for the therapeutic action of the ALS therapeutic drug riluzole is that by decreasing the excitability of neurons (Kuo et al., 2006), riluzole decreases the demand for axonal transport of cargos such as mitochondria and synaptic vesicles. Such a pharmacological action would help to compensate in the disease-related increase in necessary cooperativity. Another hypothesized pathological mechanism for which there is some experimental evidence is protein aggregation (Kieran et al., 2005; Wood et al., 2003). Protein aggregation could potentially increase the cargo sizes, via pathways such as misfolding or in the formation of dimers (Elam et al., 2003). Additionally there is the possibility for aggregation of multiple cargos into a single 'megacargo' due to the pile-up caused by slowed transport or a change in the inter-cargo distances, potentially due to changes in the stoichiometric composition of NF-H subunits (Meier et al., 1999), which normally regulates such spacing. Thus, protein aggregation would necessitate additional cooperativity, which would eventually lead to a constrained motor population unable to keep up with demand. Therefore, in summary, while cooperativity can potentially add more robustness and functionality to normal physiological transport, it can also amplify the impairments and deficits in pathological transport.

Model Limitations

Perhaps the biggest limitation of the model is that it assumes the velocity of a cargo is limited by the force imposed by the cargo (i.e. the drag force) and not by the kinetics, themselves. For example, despite the fact that the drag force is much smaller for smaller cargos (such as cargos < 200 nm diameter cargo), the kinetics could impose a limitation such that these smaller cargos travel at or about the same speed as larger cargos (i.e. there is a motor kinetically-determined maximum velocity). More generally stated, this assumption implies that the solution presented here could be non-unique in that different sets of force and kinetic contributions and/or parameters could result in the same experimentally observed velocity profiles and/or the same amount of calculated cooperativity.

Another limitation of the model is the chosen Craciun kinetic scheme, which requires that a cargo go off-track before switching directions. Very recent evidence has suggested that perhaps the cargo does not have to fully disengage from the track in order to switch directions (Muller et al., 2008). It has been proposed that the effective cargo unbinding rate decreased exponentially with the number of bound motors (Klumpp and Lipowsky, 2005). However, it is unclear if that applies only during motor over crowding or more generally. Consequently, we chose to keep the binding rate constant to maintain independent analysis of cooperativity from kinetics

Acknowledgements

This work is supported by the National Science Foundation (NSF) via a Graduate Research Fellowship and an Integrative Graduate Education and Research Traineeship Fellowship (DGE-0333411) to C.S.M. and by the Human Brain Project (NINDS, NIMH and NIBIB NS046851) to R.H.L.

References

Ashkin A, Schutze K, Dziedzic JM, Euteneuer U, Schliwa M. Force generation of organelle transport measured in vivo by an infrared laser trap. Nature 1990;348:346–8. [PubMed: 2250707]

Banks J, Carson J, Nelson B, Nicol D. Discrete-event system simulation. Pearson. 2005

Berg H. A Random Walk in Biology. Princeton. 1993

Briese M, Esmaeili B, Sattelle DB. Is spinal muscular atrophy the result of defects in motor neuron processes? Bioessays 2005;27:946–57. [PubMed: 16108074]

Brown A. Contiguous phosphorylated and non-phosphorylated domains along axonal neurofilaments. J Cell Sci 1998;111(Pt 4):455–67. [PubMed: 9443895]

Brown A. Slow axonal transport: stop and go traffic in the axon. Nat Rev Mol Cell Biol 2000;1:153–6. [PubMed: 11253369]

Brown A, Wang L, Jung P. Stochastic simulation of neurofilament transport in axons: the “stop-and-go” hypothesis. Mol Biol Cell 2005;16:4243–55. [PubMed: 16000374]

Brownlees J, Ackerley S, Grierson AJ, Jacobsen NJ, Shea K, Anderton BH, Leigh PN, Shaw CE, Miller CC. Charcot-Marie-Tooth disease neurofilament mutations disrupt neurofilament assembly and axonal transport. Hum Mol Genet 2002;11:2837–44. [PubMed: 12393795]

Coppin CM, Finer JT, Spudich JA, Vale RD. Measurement of the isometric force exerted by a single kinesin molecule. Biophys J 1995;68:242S–244S. [PubMed: 7787084]

Craciun G, Brown A, Friedman A. A dynamical system model of neurofilament transport in axons. J Theor Biol 2005;237:316–22. [PubMed: 15975597]

Elam JS, Taylor AB, Strange R, Antonyuk S, Doucette PA, Rodriguez JA, Hasnain SS, Hayward LJ, Valentine JS, Yeates TO, Hart PJ. Amyloid-like filaments and water-filled nanotubes formed by SOD1 mutant proteins linked to familial ALS. Nat Struct Biol 2003;10:461–7. [PubMed: 12754496]

Freitas R. Biocompatibility. Nanomedicine IIA. 2003

Gao YQ. A simple theoretical model explains dynein’s response to load. Biophys J 2006;90:811–21. [PubMed: 16284275]

Goldstein LS, Yang Z. Microtubule-based transport systems in neurons: the roles of kinesins and dyneins. Annu Rev Neurosci 2000;23:39–71. [PubMed: 10845058]

Gross SP, Welte MA, Block SM, Wieschaus EF. Coordination of opposite-polarity microtubule motors. J Cell Biol 2002;156:715–24. [PubMed: 11854311]

Haak RA, Kleinhans FW, Ochs S. The viscosity of mammalian nerve axoplasm measured by electron spin resonance. J Physiol 1976;263:115–37. [PubMed: 65468]

Hafezparast M, Klocke R, Ruhrberg C, Marquardt A, Ahmad-Annuar A, Bowen S, Lalli G, Witherden AS, Hummerich H, Nicholson S, Morgan PJ, Oozageer R, Priestley JV, Averill S, King VR, Ball S, Peters J, Toda T, Yamamoto A, Hiraoka Y, Augustin M, Korthaus D, Wattler S, Wabnitz P, Dickneite C, Lampel S, Boehme F, Peraus G, Popp A, Rudelius M, Schlegel J, Fuchs H, Hrabe de Angelis M, Schiavo G, Shima DT, Russ AP, Stumm G, Martin JE, Fisher EM. Mutations in dynein link motor neuron degeneration to defects in retrograde transport. Science 2003;300:808–12. [PubMed: 12730604]

Hou L, Lanni F, Luby-Phelps K. Tracer diffusion in F-actin and Ficoll mixtures. Toward a model for cytoplasm. Biophys J 1990;58:31–43. [PubMed: 2116926]

Howard J, Hudspeth AJ, Vale RD. Movement of microtubules by single kinesin molecules. Nature 1989;342:154–8. [PubMed: 2530455]

Hurd DD, Saxton WM. Kinesin mutations cause motor neuron disease phenotypes by disrupting fast axonal transport in Drosophila. Genetics 1996;144:1075–1085. [PubMed: 8913751]

Jiang YM, Yamamoto M, Kobayashi Y, Yoshihara T, Liang YD, Terao S, Takeuchi H, Ishigaki S, Katsuno M, Adachi H, Niwa J, Tanaka F, Doyu M, Yoshida M, Hashizume Y, Sobue G. Gene expression profile of spinal motor neurons in sporadic amyotrophic lateral sclerosis. Annals of Neurology 2005;57:236–251. [PubMed: 15668976]

Keller M, Tharmann R, Dichtl MA, Bausch AR, Sackmann E. Slow filament dynamics and viscoelasticity in entangled and active actin networks. Philos Transact A Math Phys Eng Sci 2003;361:699–711. [PubMed: 12871619]discussion 711–2

Kieran D, Hafezparast M, Bohnert S, Dick JR, Martin J, Schiavo G, Fisher EM, Greensmith L. A mutation in dynein rescues axonal transport defects and extends the life span of ALS mice. J Cell Biol 2005;169:561–7. [PubMed: 15911875]

Klumpp S, Lipowsky R. Cooperative cargo transport by several molecular motors. Proc Natl Acad Sci U S A 2005;102:17284–9. [PubMed: 16287974]

Kuo JJ, Lee RH, Zhang L, Heckman CJ. Essential role of the persistent sodium current in spike initiation during slowly rising inputs in mouse spinal neurones. J Physiol 2006;574:819–34. [PubMed: 16728453]

Kural C, Kim H, Syed S, Goshima G, Gelfand VI, Selvin PR. Kinesin and dynein move a peroxisome in vivo: a tug-of-war or coordinated movement? Science 2005;308:1469–72. [PubMed: 15817813]

Lupski JR. Axonal Charcot-Marie-Tooth disease and the neurofilament light gene (NF-L). Am J Hum Genet 2000;67:8–10. [PubMed: 10848490]

Marszalek JR, Williamson TL, Lee MK, Xu Z, Hoffman PN, Becher MW, Crawford TO, Cleveland DW. Neurofilament subunit NF-H modulates axonal diameter by selectively slowing neurofilament transport. J Cell Biol 1996;135:711–24. [PubMed: 8909545]

Meier J, Couillard-Despres S, Jacomy H, Gravel C, Julien JP. Extra neurofilament NF-L subunits rescue motor neuron disease caused by overexpression of the human NF-H gene in mice. J Neuropathol Exp Neurol 1999;58:1099–110. [PubMed: 10515233]

Morris RL, Hollenbeck PJ. The regulation of bidirectional mitochondrial transport is coordinated with axonal outgrowth. J Cell Sci 1993;104(Pt 3):917–27. [PubMed: 8314882]

Muller MJ, Klumpp S, Lipowsky R. Tug-of-war as a cooperative mechanism for bidirectional cargo transport by molecular motors. Proc Natl Acad Sci U S A 2008;105:4609–14. [PubMed: 18347340]

Pantelidou M, Zographos SE, Lederer CW, Kyriakides T, Pfaffl MW, Santama N. Differential expression of molecular motors in the motor cortex of sporadic ALS. Neurobiol Dis 2007;26:577–89. [PubMed: 17418584]

Rao MV, Nixon RA. Defective neurofilament transport in mouse models of amyotrophic lateral sclerosis: a review. Neurochem Res 2003;28:1041–7. [PubMed: 12737529]

Sabry J, O'Connor TP, Kirschner MW. Axonal transport of tubulin in Ti1 pioneer neurons in situ. Neuron 1995;14:1247–56. [PubMed: 7541635]

Schmitz KA, Holcomb-Wygle DL, Oberski DJ, Lindemann CB. Measurement of the force produced by an intact bull sperm flagellum in isometric arrest and estimation of the dynein stall force. Biophys J 2000;79:468–78. [PubMed: 10866972]

Shea TB, Flanagan LA. Kinesin, dynein and neurofilament transport. Trends Neurosci 2001;24:644–8. [PubMed: 11672808]

Teuchert M, Fischer D, Schwalenstoecker B, Habisch HJ, Bockers TM, Ludolph AC. A dynein mutation attenuates motor neuron degeneration in SOD1(G93A) mice. Exp Neurol 2006;198:271–4. [PubMed: 16427626]

Trivedi N, Jung P, Brown A. Neurofilaments switch between distinct mobile and stationary states during their transport along axons. J Neurosci 2007;27:507–16. [PubMed: 17234583]

Truskey, G.; Yuan, F.; Katz, D. Transport Phenomena in Biological Systems. Prentice Hall; 2003.

Visscher K, Schnitzer MJ, Block SM. Single kinesin molecules studied with a molecular force clamp. Nature 1999;400:184–9. [PubMed: 10408448]

Wagner OI, Ascano J, Tokito M, Leterrier JF, Janmey PA, Holzbaur EL. The interaction of neurofilaments with the microtubule motor cytoplasmic dynein. Mol Biol Cell 2004;15:5092–100. [PubMed: 15342782]

Wang L, Brown A. Rapid intermittent movement of axonal neurofilaments observed by fluorescence photobleaching. Mol Biol Cell 2001;12:3257–67. [PubMed: 11598207]

Wang L, Ho CL, Sun D, Liem RK, Brown A. Rapid movement of axonal neurofilaments interrupted by prolonged pauses. Nat Cell Biol 2000;2:137–41. [PubMed: 10707083]

Wood JD, Beaujeux TP, Shaw PJ. Protein aggregation in motor neurone disorders. Neuropathol Appl Neurobiol 2003;29:529–45. [PubMed: 14636160]

Yoo J, Kambara T, Gonda K, Higuchi H. Intracellular imaging of targeted proteins labeled with quantum dots. Exp Cell Res. 2008

Zhang F, Strom AL, Fukada K, Lee S, Hayward LJ, Zhu H. Interaction between familial amyotrophic lateral sclerosis (ALS)-linked SOD1 mutants and the dynein complex. J Biol Chem 2007;282:16691–9. [PubMed: 17403682]

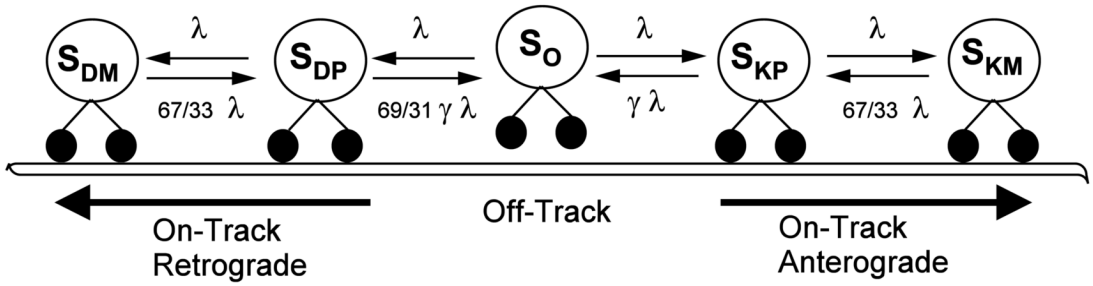

Figure 1.

The motor-microtubule binding kinetics are adapted from Craciun et al (Craciun et al., 2005). The model contains five states, *S*, which are differentiated using the following subscript nomenclature: *P* represents a paused motor (i.e. $V = 0$), *M* represents a moving motor (i.e. $V > 0$), *K* represents the molecular motor kinesin, *D* represents the molecular motor dynein, and *O* represents an off-track motor. Using this nomenclature, we obtain the following states: S_O) off-track, paused; S_{KP}) kinesin, on-track, paused; S_{DP}) dynein, on-track, paused; S_{KM}) kinesin, on-track, moving anterogradely; S_{DM}) dynein, on-track, moving retrogradely. Rate constants are shown in parameter-form as given in Craciun et al (Craciun et al., 2005). The tuned slow transport rate parameters are $\gamma = 2.5$ and $\lambda = 0.1$. Fast transport rate parameters are $\gamma = 0.2$ and $\lambda = 10$. For details regarding the derivation of rate constants and equations, see Craciun et al (Craciun et al., 2005).

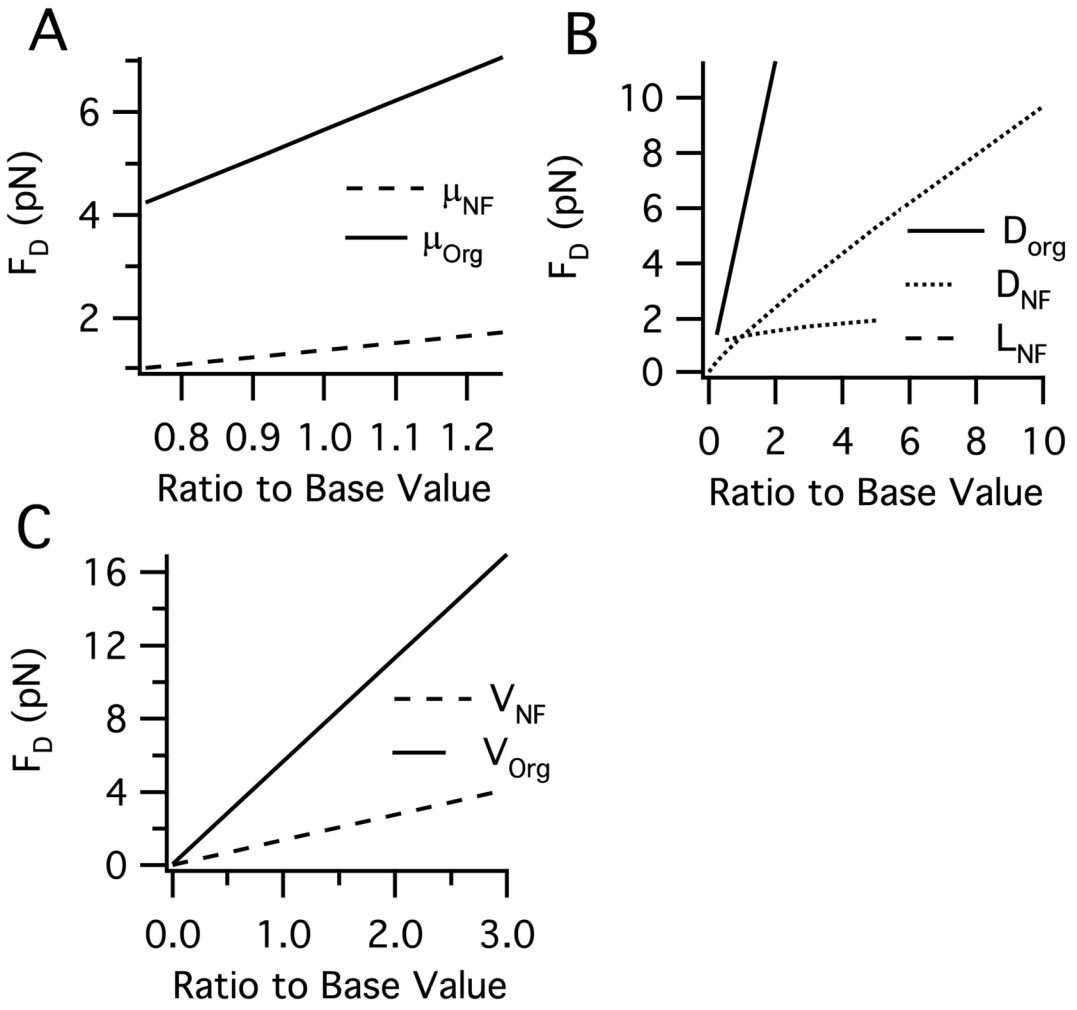

Figure 2.
Range of drag force (F_D) over physiologically relevant parameter ranges for cytoplasmic viscosity (μ), cargo geometry, and cargo transport velocity (*V*) as listed in Table 2 for both a neurofilament and an organelle. The x-axis 'ratio to base value' refers to the ratio of the base parameter value given in Table 2. **A**. Effect of cytoplasmic viscosity. **B**. Effect of cargo geometry: the diameter and length of a cylindrical neurofilament (D_{NF}) and the diameter of a spherical organelle (D_{Org}). **C**. Effect of cargo velocity.

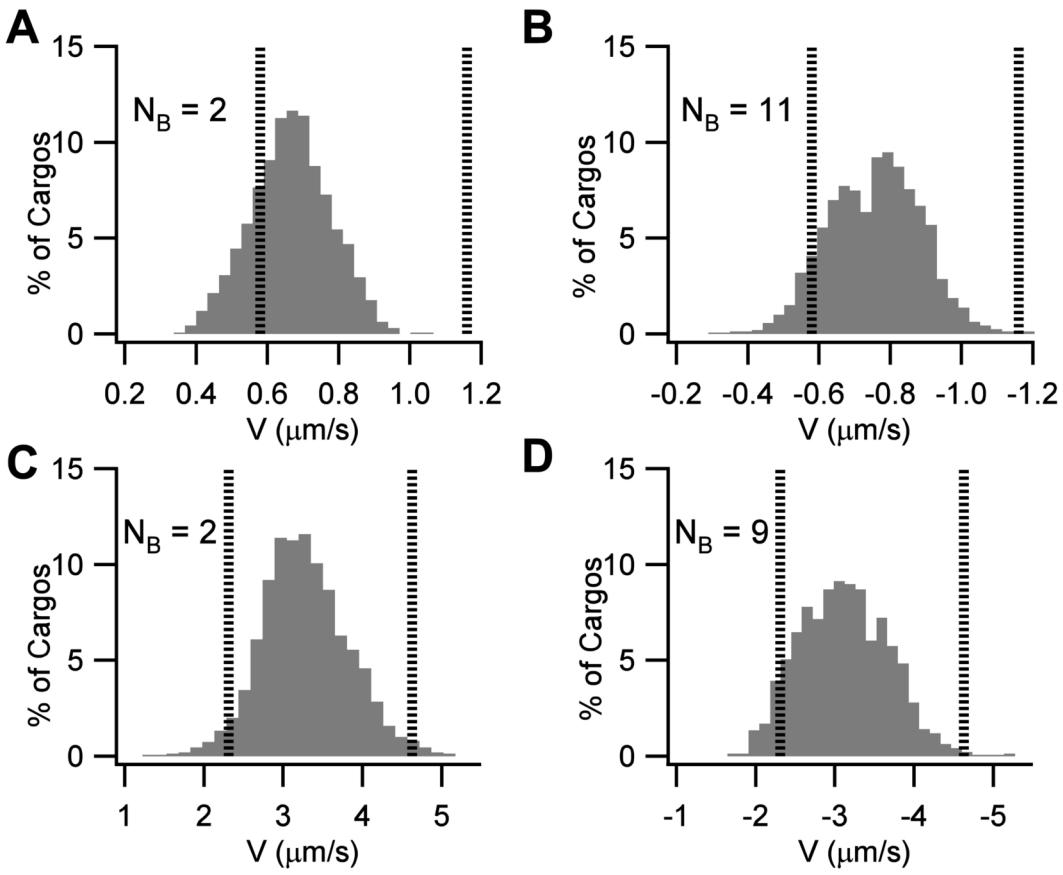

Figure 3.

Velocity distributions over fast axonal transport ranges. Anterograde transport by kinesin is represented by a positive sign convention while retrograde transport by dynein is represented by a negative sign convention. The distributions represent the average velocity of a population of cargos over the 4.74 second simulated period. The figure represents the minimum number of bound motors (N_B) required to obtain a population of cargos whose average velocity is approximately centered at the average of the experimental ranges shown in Table 1. Vertical lines represent the edges of the experimental velocity ranges shown in Table 1. The ordinate indicated the normalized percentage of cargos which fall within each velocity bin. **A**. Anterograde populations of 1μm spherical cargos representative of the 'bi-directional' transport range of ~0.58–1.16 μm/s (e.g. 50–100 mm/day) require greater than 2 bound kinesin motors per cargo. **B**. Retrograde populations of 1μm spherical cargos representative of the 'bidirectional' transport range of 0.58–1.16 μm/s (e.g. 50–100 mm/day) require 11 bound dynein motors. **C**. Anterograde populations of 200 nm spherical cargos representative of the fast transport range of ~2.31–4.63 μm/s (e.g. 200–400 mm/day) is obtained by a minimum of 2 bound kinesin motors per cargo. **D**. Retrograde populations of 200 nm spherical cargos representative of the fast transport range of ~2.31–4.63 μm/s (e.g. 200–400 mm/day) is obtained by a minimum of 9 bound dynein motors per cargo.

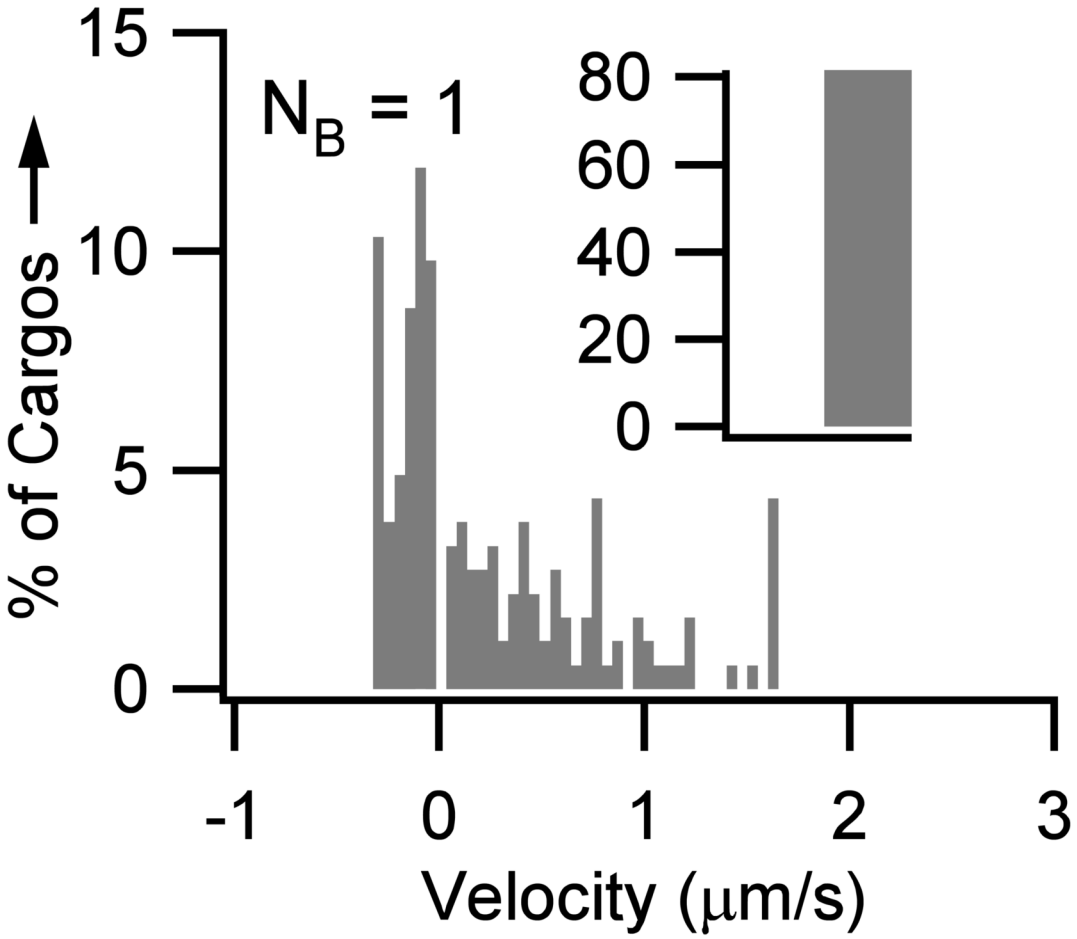

Figure 4.
Slow transport of neurofilaments. To obtain an experimentally equivalent velocity profile for slow transport of neurofilaments, no cooperativity is required. That is, only one bound motor is needed per cargo. The figure shows the velocity histogram of a population of average-sized neurofilaments (L_{NF} =1.6 μm and D_{NF} = 10 nm). Note that for visual clarity the zero velocity bin (0 μm/s) as been moved to the inset. Thus, the inset shows the number of cargos that remained paused during the length of the simulation (i.e. ~83% of cargos had velocities equal to 0 μm/s over the 4.74 second simulated period, similar to the 85% seen experimentally (Brown et al., 2005)).

Table 1

Experimentally determined transport ranges and known/hypothesized transport types (adapted from Brown (Brown, 2000)).

Transport Type	Velocity (mm/day)	Velocity (μm/s)	Example Cargo Type(s)
Fast			
--Anterograde	200–400	2.31–4.63	Golgi-derived vesicles, tubules, neurotransmitters
--Retrograde	200–400	2.31–4.63	enodosomes, lysosomes
--Bidirectional	50–100	0.58–1.16	mitochondria
Slow			
--Component A	0.3–3	0.003–0.035	neurofilaments
--Component B	2–8	0.02–0.08	microfilaments, actin

Table 2

Base parameter values, ranges, and references used for calculating drag force. Note that the higher end of the neurofilament diameter range includes side arms, and that viscosity is that of measurements which include the cytoplasmic protein network in addition to the cytoplasmic fluid itself.

Parameter Name	Base	Primary Physiological Range	Primary References
Viscosity, μ (Poise)	6	unknown (see Methods)	(Keller et al., 2003)
Neurofilament length, L_{NF} (μm)	1.6	1–3	(Trivedi et al., 2007; Wagner et al., 2004)
Neurofilament diameter, D_{NF} (nm)	10	10–50	(Marszalek et al., 1996)
Organelle diameter, D_{Org} (nm)	1	200–2000	(Freitas, 2003)
Velocity, v (μm/s)	1	0.25–3	(Brown et al., 2005; Klumpp and Lipowsky, 2005; Kural et al., 2005; Visscher et al., 1999)

Table 3

Number of bound motors (N_B) required for various experimentally determined fast transport speeds and cargo sizes. For experimental range categories, refer to Table 1.

Average Velocity (mm/day)	Average Velocity (mm/s)	Cargo Diameter (nm)	N_B Retro-grade	N_B Antero-grade
50–100	0.58–1.16	500	5–7	1–2
50–100	0.58–1.16	1000	11–14	2–3
200–400	2.31–4.63	200	9–12	2–3
200–400	2.31–4.63	300	12–15	3–4
200–400	2.31–4.63	500	26–30	6–8